Study of Phase and Patterns Characteristics of a Sub-Wavelength Broadband Reflectarray Unit Element Based on Triple Concentric Circular-Rings

Javad Nourinia, Changiz Ghobadi, Bahman Mohammadi, and Farzad Alizadeh

Department of Electrical Engineering
Urmia University, Urmia, WA 5756151818, Iran
{j.nourinia, ch.ghobadi, b.mohammadi, fa.alizadeh}@urmia.ac.ir

***Abstract*—**In this paper, phase and patterns characteristics of a sub-wavelength broadband reflectarray (RA) unit element are propounded. The unit element consists of triple concentric circular-rings on the Rogers 4003 substrate (H_2) that provide a nearly 615˚ linear phase range. To obtain a phase curve with a lower slope, a 3 mm thick Foam (H_1) is used and backed by a ground plane. A complete investigation analysis has been done to study the phase and patterns characteristics of the proposed sub-wavelength RA unit element. Results indicate that not only the incidence angle alter the element reflection phase, but also for oblique incidence, the element pattern deforms. It is shown, for sub-wavelength elements the combined effects of the mentioned factors are less severe.

***Index Terms* —** Broadband, concentric rings, patterns characteristics, unit element.

I. INTRODUCTION

A microstrip RA antenna consists of an array of microstrip patches and an illuminating feed antenna [1]-[3]. In the design of RA antenna, one of the most important issues is to achieve a phase shift of more than 360° to insure the required phase compensation. Different variations of phasing methods for a microstrip RA have been introduced. These include multilayer stacked patches [1], aperture coupled designs [1] and single layer multi-resonant elements [2].

II. DEISGN & CONFIGURATION

The layout of the proposed unit element is displayed in Fig. 1. The phase-shift mechanism is obtained by variation of diameter of rings. It consists of three concentric circular rings, where the radius of inner side of the ring is equal to the radius of the outer side of the ring multiplied by the factor of K_i. These elements are etched on a substrate with permittivity (ε_r) of 3.55 and thickness (H_2) of 0.813 mm. An element spacing of 15 mm (0.5 λ_0 at 10 GHz) is used to avoid grating lobes. To obtain a smoother phase curve, a Foam gap (H_1=3 mm) is considered between the substrate and the ground plane [4]. All the optimized parameters are specified as follows: $K_1 = 0.25$, $K_2 = 0.4$, $K_3 = 0.55$, $K_4 = 0.7$, $K_5 = 0.85$, $D = 2R$.

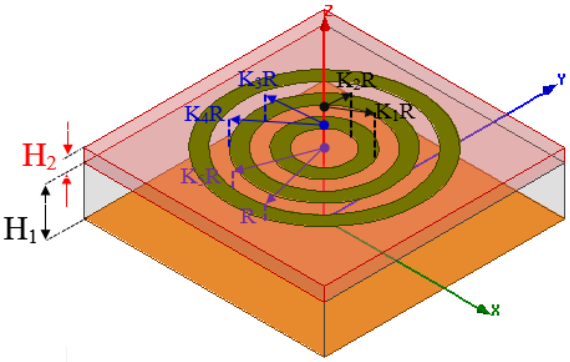

Fig. 1. Geometry of the triple concentric circular-rings.

In [5] and [6], four parameters presented to investigate the element efficiency. In this paper, we further dig into the range (ψ) and variation (β) of the reflection phase that affects the directivity [1]; the sensitivity to fabrication tolerances (σ) that affects the quantization errors [3]; and the phase variation rate versus frequency of the phase curve relative to the RA elements (α, dispersion [2]) that influences the gain bandwidth [6]. In this work, the polarization of the incident and reflected waves are the θ-polarized, that have the electric fields parallel to the plane of incidence (x-z plane) with E_x and E_z components and the magnetic field transverse to it (TM case) [7]. The mode to consider this scanning is the TM_{00} mode which is the zeroth-order Floquet modes and, therefore, the conventional plane wave [1].

In Fig. 2, the phase responses are plotted for λ/2 unit-element. Figure 2 (a) shows that incorporating of multi-resonance elements eases to reach wide range phase. Here, the bandwidth of the designed RA element is defined based on the evaluation of the frequency range by normalizing all the curves with respect to the central frequency (10 GHz), apart from a margin error $\Delta\psi$ which equals to ±45˚ [5]. As it can be observed, the resulting

Submitted On: January 27, 2017
Accepted On: September 22, 2017

bandwidth is equal to the value of about 6%, where the lower (9.7 GHz) and upper (10.3 GHz) bounds of bandwidth can be identified by dashed lines on Fig. 2 (c). Also, the bandwidth can be obtained by the frequency range within which all the phase curves computed for different values of the element size D are almost parallel [6].

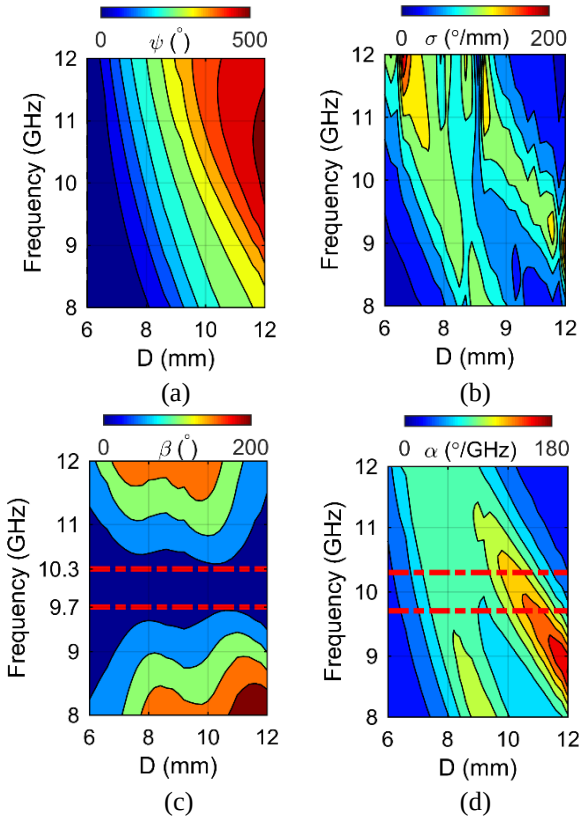

Fig. 2. The reflection phase characteristics of the λ/2 unit-element: (a) ψ, (b) σ, (c) β, and (d) α.

III. RESULTS & DISCUSSION

All elements in the RA must have proper spacing between adjacent elements in order to avoid the grating lobes in the radiation pattern. The element spacing should be governed by the following conventional array equation [1, 8]:

$$\frac{d}{\lambda} \le \frac{1}{\sqrt{\varepsilon_r} + \sin\theta}, \tag{1}$$

where d is the element spacing or unit cell size, ε_r is the relative dielectric constant and θ is either the incident angle from the feed or the main beam tilt angle from the broadside direction, whichever is larger. λ is the free-space wavelength of the highest frequency in the application. Offset-fed reflectarrays are more prone to grating lobe formation, in case the element spacing is much larger than 0.5 λ_0.

Another fundamental scanning property typical of phased arrays is known as scan blindness. It is caused by the resonance phenomenon that occurs when surface waves are excited in synchronism with the Floquet modes of the periodic structure [9]-[10]. Scan angle depends on the substrate thickness, the substrate relative permittivity and the inter-element spacing. The scan blindness occurs before the onset of the grating lobe, requiring the re-calculation of the element spacing to maintain keeping the scan blindness out of the required scanned area. The presence of the TM_0 surface wave causes scan blindness only in the E-plane [10]. The approximate angle at which scan blindness occurs is closer to broadside by the angle θ_{sc}, where

$$\theta_{SC} = \sin^{-1}\left(\frac{\beta_{SW}}{\kappa_0} - 1\right), \tag{2}$$

where θ_{sc} is the difference in angle between the onset of the grating lobe (1) and scan blindness, β_{sw} is the propagation constant of the surface wave TM_0, and K_0 is the free-space propagation constant. The value of the propagation constant for the dominant surface wave mode, TM_0, in a grounded-dielectric substrate, is given by the first root of the function $T_m(\beta)$ [9]. The implication of the phenomenon of scan blindness is to force a re-calculation of the element spacing, such that the scan blindness is out of the required scan area.

To improve the gain bandwidth of the structure [6, 11] and lower quantization phase error [3], sub-wavelength unit elements have been presented that have sizes and periodicity below the typical λ/2 spacing. In Fig. 3, the phase response is plotted for λ/4 unit-element. It is evident (Fig. 3 (a)) that the achievable reflection phase range decreases with spacing reduction. It is noticed in Fig. 3 (b) that the phase curves feature more linear behavior and are less sensitive to the size variation with the decrease of the element spacing [11]. Therefore, a good manufacturing tolerance is expected to be obtained with sub-wavelength elements. An impressive bandwidth improvement, from 6% to 13% around the design frequency f_0=10 GHz, is observed when decreasing the inter-element spacing from $0.5\lambda_o$ to $0.25\lambda_o$. Notice also the obvious similarity between the sensitivity to size (Fig. 3 (b)) and frequency dependency of dispersion (Fig. 3 (d)) in sub-wavelength element, confirming that dispersion and fabrication tolerance are deeply associate quantities. There is a similar lower sensitivity to the incidence angle of the incoming wave for the reduced spacing, as can be gleaned from Figs. 4 (a) and (b), which apply to the $\varphi_{inc} = 0^\circ$ case. The λ/2 spacing case in Fig. 4 (a) is more dependent on the value of the θ_{inc} than the reduced spacing λ/4 case in Fig. 4 (b), for large incidence angles [7].

Figures 5 (a)-(c) show the element patterns characteristics for different values of inter-element spacing at different frequencies. It can be seen that the

variations of element patterns for H-plane (y-z plane) are larger than E-Plane (x-z plane) case. Clearly, such variations are smaller for sub-wavelength RA elements than half-wavelength ones. It can be gleaned from Fig. 5, that the element pattern at H-plane for sub-wavelength case is more dependent on the value of the frequency. This observation stems from the fact that at frequencies below 10 GHz (the center-frequency), like 9 GHz, the element spacing becomes a smaller fraction of the wavelength compared to what it is at 10 GHz.

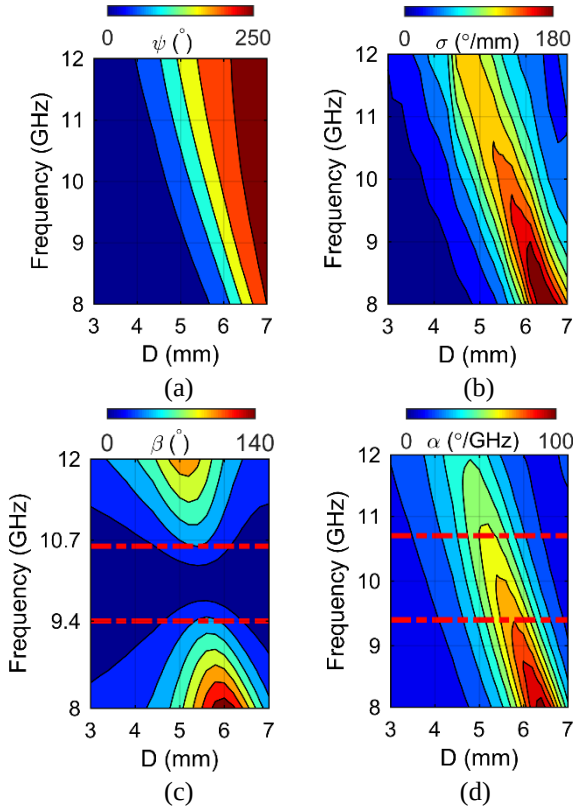

Fig. 3. The reflection phase characteristics of the λ/4 unit-element: (a) ψ, (b) σ, (c) β, and (d) α.

Figures 6 (a)-(b) show the element patterns characteristics for different values of inter-element spacing at different oblique incidence angles. It is immediately noticed that there is a narrowing of the element beamwidth when θ_{inc} increases from zero. Furthermore, the element pattern becomes deformed. Both beamwidth narrowing and deformation effects become less severe for the sub-wavelength lattice situation, therefore, one more reason for the superior behavior of sub-wavelength reflectarrays. The element patterns are important both from the point of view of coupling of the feed field to the elements, and the reradiated field from the elements [7].

The current amplitude distribution in the substrate region below the ring elements, at different frequencies is displayed in Fig. 7, when it is excited by an x-pol plane wave at normal incident angle for the element with different inter-element spacing. It can be noticed that the intense resonation occurs alongside the gap between the inner and outer rings [12]. In [12], it is shown that these radiating edges act as secondary sources and reradiates the required reflection phase. It is also observed that at λ/2 unit elements these currents are more dominant than at λ/4 sizes which indicates that the sub-wavelength unit elements have lower loss and more total performance [11-12].

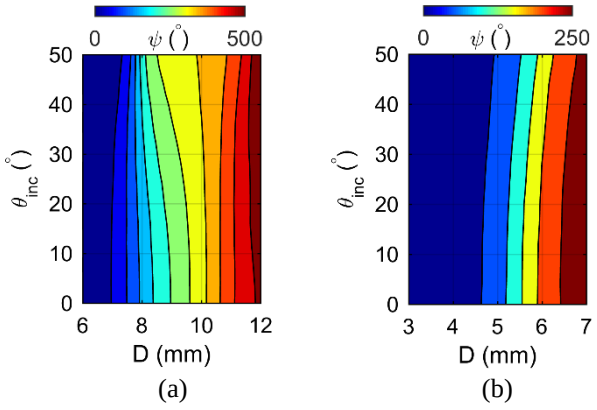

Fig. 4. The reflection phase characteristics at 10 GHz: (a) λ/2 unit-element, and (b) λ/4 unit-element.

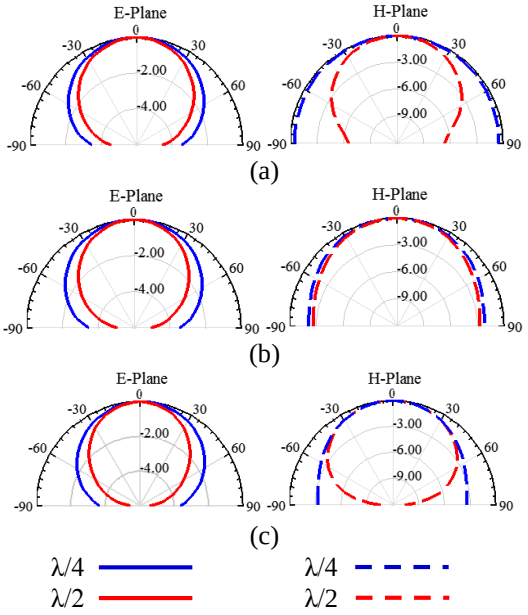

Fig. 5. Element patterns for different inter-element spacing: (a) 9 GHz, (b) 10 GHz, and (c) 11 GHz.

IV. CONCLUSION

In this paper, a sub-wavelength broadband RA unit element based on triple concentric circular-rings is evaluated. A complete investigation has been done

to study the phase and patterns characteristics of the proposed sub-wavelength RA unit element for oblique incidence angles. It is shown that the incidence angle alters the element reflection phase and the element patterns, but for sub-wavelength elements these effects are less intensive.

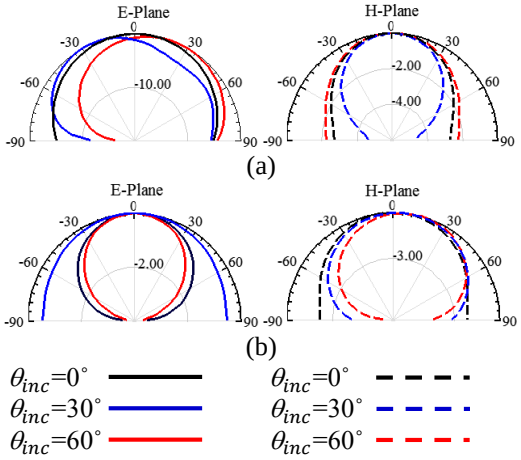

Fig. 6. Element patterns for different θ_{inc}: (a) λ/2 unit-element, and (b) λ/4 unit-element.

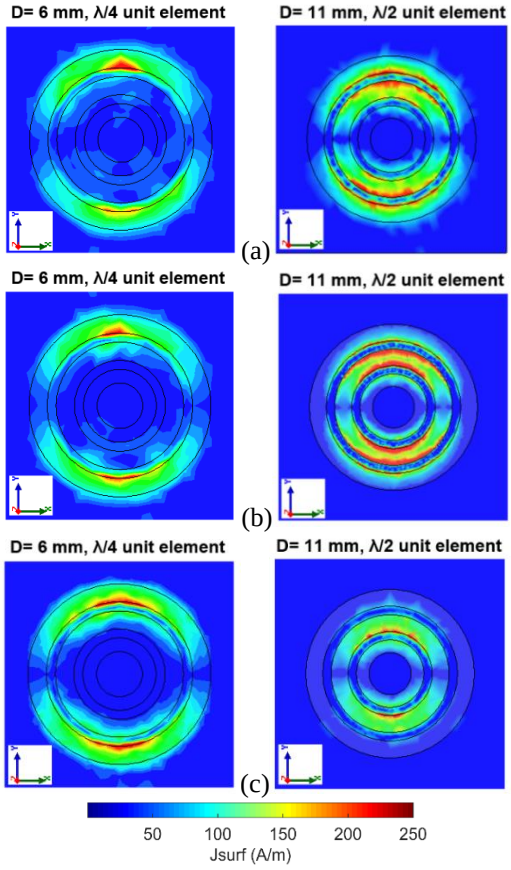

Fig. 7. Current distribution for normal incidence at: (a) 9 GHz, (b) 10 GHz, and (c) 11 GHz.

REFERENCES

[1] J. Huang and J. A. Encinar, *Reflectarray Antennas*. New York: IEEE/John Wiley & Sons, 2008.

[2] J. Shaker, M. R. Chaharmir, and J. Ethier, *Reflectarray Antennas, Analysis, Design, Fabrication, and Measurement*. Boston, London: Artech House, 2013.

[3] P. Nayeri, F. Yang, and A. Z. Elsherbeni, *Reflectarray Antennas: Theory, Designs, and Applications*. IEEE-Wiley, 2017.

[4] M. E. Bialkowski and K. H. Sayidmarie, "Investigations into phase characteristics of a single-layer reflectarray employing patch or ring elements of variable size," *IEEE Trans. Antennas and Prop*., vol. 56, no. 11, pp. 3366- 3372, Nov. 2008.

[5] M. Bozzi, S. Germani, and L. Perregrini, "Performance comparison of different element shapes used in printed reflectarrays," *IEEE Antennas and Wireless Prop. Letters*, vol. 2, pp. 219-222, 2003.

[6] F. Venneri, S. Costanzo, and G. Di Massa, "Bandwidth behavior of closely spaced aperture-coupled reflectarrays," *International Journal of Antennas and Propagation*, vol. 2012, Article ID 846017, July 2012.

[7] E. R. F. Almajali and D. A. McNamara, "Angle of incidence effects in reflectarray antenna design: Making gain increases possible by including incidence angle effects," *IEEE Antennas and Propagation Magazine*, vol. 58, no. 5, pp. 52-64, Oct. 2016.

[8] Y. Fujii, K. Ikarashi, Sh. Makino, T. Hirota, K. Noguchi, and K. Itoh, "High-efficiency and low-side-lobe reflectarray antenna," *Proceedings of ISAP 2014*, Kaohsiung, Taiwan, Dec. 2-5, 2014.

[9] D. M. Pozar and D. H. Schaubert, "Scan blindness in infinite phased arrays of printed dipoles," *IEEE Trans. Antennas Propag*., vol. 32, pp. 602-610, June 1984.

[10] P. D. Patel, "Approximation location of scan-blindness angle in printed phased arrays," *IEEE Antennas and Propagat. Magazine*, vol. 34, pp. 53-54, Oct. 1992.

[11] P. Nayeri, F. Yang, and A. Z. Elsherbeni, "Bandwidth improvement of reflectarray antenna using closely spaced elements," *PIER*, vol. 18, pp. 19-29, 2011.

[12] H. Rajagopalan, S. Xu, and Y. Rahmat-Samii, "On understanding the radiation mechanism of reflectarray antennas: An insightful and illustrative approach," *IEEE Antennas and Propagation Magazine*, vol. 54, no. 5, pp. 14-38, 2012.